Proc. Indian Acad. Sci. (Chem. Sci.), Vol. 103, No. 3, March 1991, pp. 283–293.

From femtoseconds to biology: Mechanism of bacteriorhodopsin's light-driven proton pump

RICHARD A MATHIES
Chemistry Department, University of California, Berkeley, CA 94720, USA

Abstract. Bacteriorhodopsin is a retinal-containing protein that functions as a light-driven proton pump. Resonance Raman and femtosecond dynamic absorption spectroscopy are being used to elucidate the molecular mechanism of bacteriorhodopsin. The primary photochemical process is a *trans*-to-*cis* isomerization about the C_{13}=C_{14} bond of the retinal chromophore that has been directly observed using femtosecond dynamic absorption spectroscopy. The excited state isomerization dynamics can be quantitatively analyzed using a new theory for nonstationary state spectroscopy. Resonance Raman vibrational spectroscopy has been used to determine the structure of the chromophore in each of bacteriorhodopsin's intermediates and to analyze the kinetics of the photocycle. These results are integrated into an explicit molecular model (the C–T Model) for proton pumping in bacteriorhodopsin.

Keywords. Purple membrane; femtosecond spectroscopy; resonance Raman spectroscopy; nonstationary state spectroscopy.

1. Introduction

Bacteriorhodopsin (BR) is an intrinsic membrane protein, found in the purple membrane of *Halobacterium halobium*, that functions as a light-driven proton pump (Birge 1990; Khorana 1988). BR contains an all-*trans* retinal chromophore bound to the protein as a protonated Schiff base. The primary action of light is to isomerize the chromophore to 13-*cis* thereby activating the protein and causing it to pump protons across the cell membrane (see figure 1). We want to understand the molecular mechanism of this process from the initial femtosecond torsional events in the excited electronic state of BR_{568} to the protein structural changes that translocate protons. To study the femtosecond isomerization events, we have performed 6-femtosecond dynamic absorption spectroscopy (Mathies *et al* 1988), and have developed a new theory for femtosecond nonstationary state spectroscopy which permits the quantitative analysis of these data (Pollard *et al* 1990a, b). To understand the later events that lead to proton pumping, we have used resonance Raman spectroscopy to determine the structure of the retinal chromophore in each of bacteriorhodopsin's intermediates (Mathies *et al* 1987). Monitoring the intensity of the scattering from each intermediate as a function of time permitted the quantitative analysis of the kinetics of the photocycle (Ames and Mathies 1990). These data have been used to formulate the C–T Model for proton pumping (Fodor *et al* 1988). An explicit molecular graphics model for the events in the photocycle will be presented.

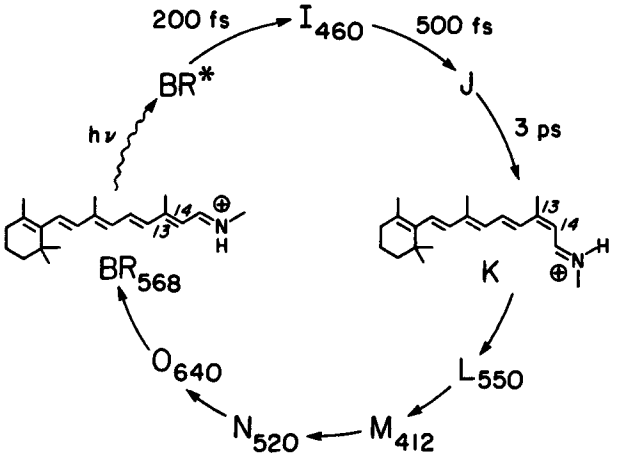

Figure 1. Kinetic scheme for the light-driven proton-pumping photocycle of bacteriorhodopsin.

2. Nonstationary state theory for femtosecond spectroscopy

The large spectral width of ultrashort 6-fs optical pulses makes possible pump-probe experiments which measure the complete time-resolved absorption spectrum with high resolution in both frequency and time. To provide a quantitative analysis of these data, we have formulated the perturbative density matrix theory for the third order susceptibility of a multi-level system in terms of four-time correlation functions which can be interpreted as the time-dependent overlap of bra and ket vibrational wavepackets propagating independently on the ground and excited state electronic potential surfaces (Pollard *et al* 1990b). When vibrational motion during the excitation is minimal, or when the pump pulse is much shorter than the optical T_2, then the probe pulse interrogates an essentially pure state. In this case, the dynamic absorption spectrum represents the *first-order* spectroscopy of the *non-stationary* initial state created by the pump pulse, $|\psi_1(t)\rangle$, according to

$$\sigma(\omega) \propto \omega \,\mathrm{Im}\,\{\mathbf{P}^{(1)}_{pr}(\omega)/\mathbf{E}_{pr}(\omega)\}, \tag{1}$$

$$P^{(1)}_{pr}(t) = \langle\psi_1(t)|\mu^*_{21}|\psi_2(t)\rangle, \tag{2}$$

where

$$|\psi_2(t)\rangle = \frac{i}{\hbar}\int_{-\infty}^{t} dt' e^{-\gamma_{21}(t-t')} e^{-i\mathbf{h}_2(t-t')/\hbar}\mu_{21} E_{pr}(t')|\psi_1(t')\rangle, \tag{3}$$

is the wavefunction created on the final state by the probe pulse. Here, $\mathbf{E}_{pr}(\omega)$ and $\mathbf{P}_{pr}(\omega)$ are the Fourier transforms of the electric field of the probe and the system polarization induced by the pulse; $\mathbf{h}_1$ and $\mathbf{h}_2$ are the vibrational Hamiltonians of the initial and final electronic states, which are coupled by the transition dipole μ_{21} and whose superposition is dephased at the rate γ_{21}. The relevant correlation function represents the time-dependent matrix element of μ_{21} between the time-evolving initial wavefunction and the wavepacket created on the final state by the probe pulse.

2.1 *Model calculation for harmonic potentials*

Figure 2 presents model calculations of stimulated emission spectra when the ground and excited state surfaces have equal 500 cm^{-1} vibrational frequencies. After delta function pulse excitation, the excited state wavepacket moves back and forth with a period of 67 fs. This is the femtosecond nonstationary state that we want to study. It may be interrogated through excited state absorption or stimulated emission. After a time delay of 15 fs, the depicted probe pulse projects a copy of the wavepacket down on the ground state potential surface and the subsequent evolution of both the ground and excited state wavepackets is shown. The transient stimulated emission spectra for this case are shown in figure 3. At zero time delay, the excited state wavepacket has not had a chance to move from the Franck–Condon region and the emission is identical to the ground state absorption. From 5–30 fs the emission shifts down to lower energies following the decrease in the energy gap as the wavepacket moves towards the far turning point. From 35 to 65 fs the excited state wavepacket returns to the Franck–Condon region and this is manifested in the shift of the emission maximum back toward 0 cm^{-1}. Excited state absorption is treated in exactly the same way except that the probe pulse creates a copy of the nonstationary S_1 wavepacket on the S_n surface. The overall differential transmittance spectrum is the sum of the stimulated emission, excited state absorption, and dynamic ground state hole as has recently been discussed in detailed analyses of Nile Blue (Pollard *et al* 1990a).

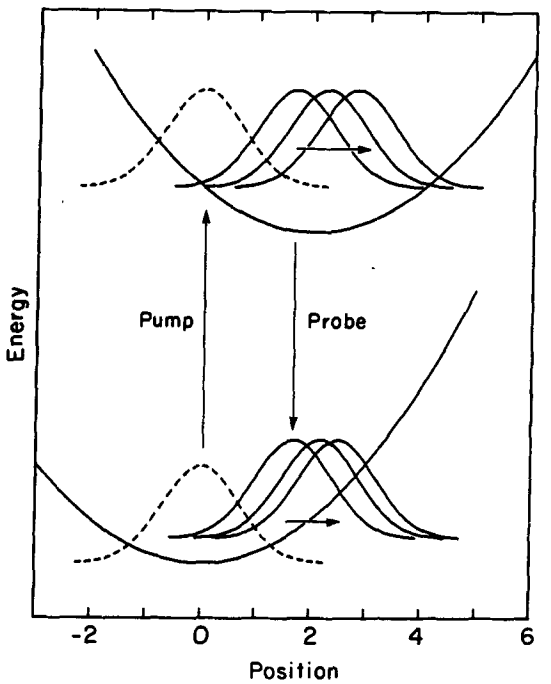

Figure 2. Potential surfaces and wavepacket dynamics for 500 cm^{-1} harmonic ground and excited states (dimensionless displacement of 2). The figure depicts the ground and excited state wavepacket dynamics following a δ-function probe pulse 15 fs after excitation.

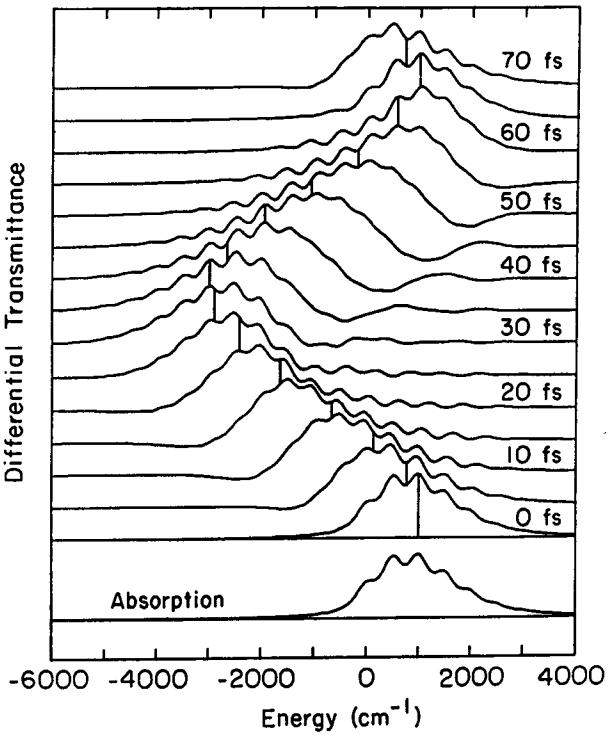

Figure 3. Excited state stimulated emission contribution to the differential transmittance spectra for the potential surfaces in figure 2.

2.2 *Analysis of bacteriorhodopsin isomerization dynamics*

As an example of femtosecond spectroscopy using finite pulses and anharmonic surfaces, we present an analysis of the femtosecond dynamic absorption spectra of the excited state *trans*→*cis* torsional isomerization of the retinal chromophore in bacteriorhodopsin (Mathies *et al* 1988). The differential transmittance spectra given in figure 4 were calculated from the time-dependent wavepackets in figure 5 using (1)–(3). For the anharmonic surfaces and finite pulses required in this system, the equations were evaluated by numerical wavepacket propagation using the fast Fourier transform second-order differencing algorithm of Kosloff (1988). In the first ~ 200 fs we observe both a relatively sharp excited state absorption feature at 580 nm which broadens and blueshifts with time, and a very broad stimulated emission band from 640–700 nm which grows in and decays in the red. Since both of these bands arise from the same initial excited state wavepacket, the differences between them must reflect the unique differences between the final electronic potential surfaces for each transition, i.e., S_0 for the emission band and S_n for the absorption band. In this one-dimensional model, the width of the ground state absorption is due to the steep slope of the S_1 surface in the Franck–Condon region. The much greater breadth of the stimulated emission band, as compared to the ground state depletion band, simply reflects the spreading of the excited state wavepacket during its preparation by the long 60 fs pump pulse. The rapid disappearance of emission comes from the drop in the S_0–S_1 energy gap as the wavepacket moves towards the excited state minimum

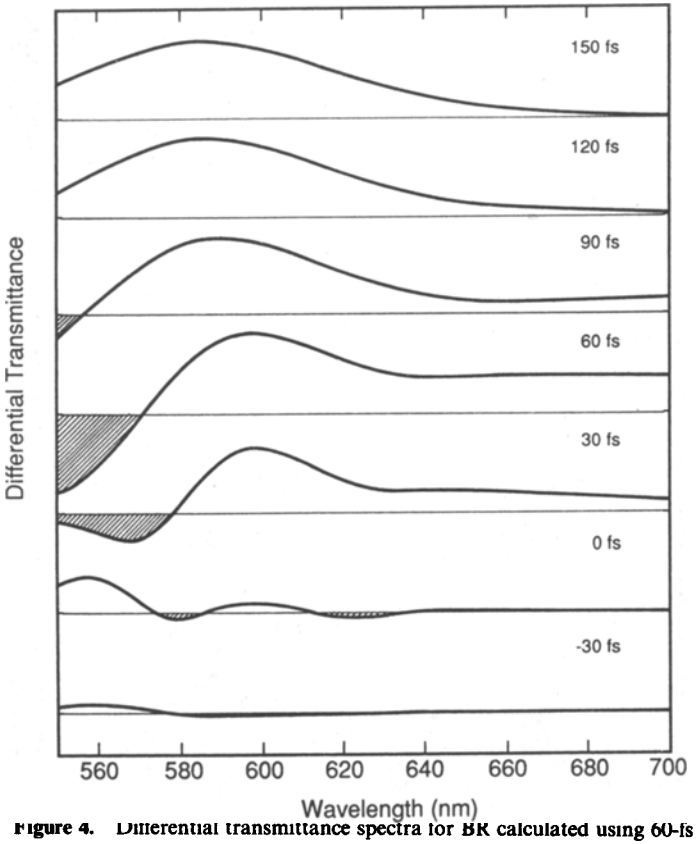

Figure 4. Differential transmittance spectra for BR calculated using 60-fs pump and 6-fs probe pulses and the potential surfaces of figure 5 (Pollard *et al* 1990b).

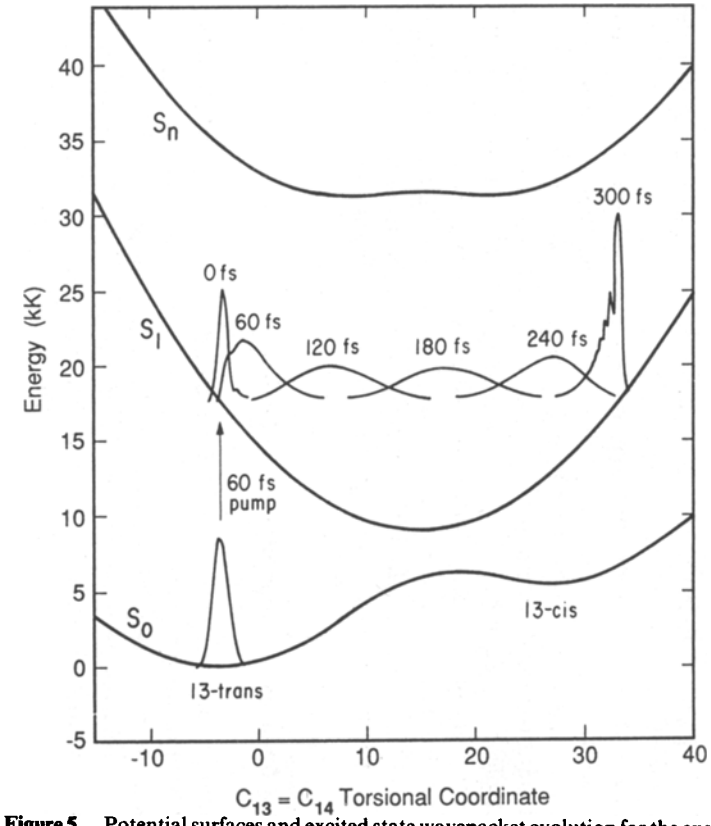

Figure 5. Potential surfaces and excited state wavepacket evolution for the excited state *trans*→*cis* isomerization of BR_{568} (Pollard *et al* 1990b). The wells in the S_0 and S_1 states are 50 cm^{-1} harmonic surfaces, the $S_0 \rightarrow S_1$ energy gap at the ground state minimum was set to give a ground state absorption maximum of 568 nm; the $S_1 \rightarrow S_n$ energy gap was set to 580 nm at the ground state minimum, and to 460 nm at the S_1 state minimum, in order to reproduce the observed behaviour of the excited state absorption feature.

(and the ground state isomerization barrier). The much sharper excited state absorption feature then reveals that the S_1 and S_n surfaces must have very similar slopes in the Franck–Condon region, so that the variation of the $S_1 \rightarrow S_n$ energy gap over the wavepacket is limited.

The excellent qualitative agreement between the calculated spectra of figure 4 and experimental spectra up to ~ 150 fs argues strongly for the correctness of our original interpretation, that the experiments directly reflect coherent wavepacket evolution on the excited state torsional potential surface of BR_{568} (Mathies *et al* 1988). The sharp transient bleaching found at the pump wavelength in the first ~ 60 fs is due to a coherent coupling of the pump and probe pulses which occurs whenever they overlap in time (Pollard *et al* 1988). Here, we have shown that all the other significant features of the bacteriorhodopsin experiments can be accurately described in terms of the coherent *intramolecular* dynamics of the reacting molecule.

3. Resonance Raman spectroscopy of bacteriorhodopsin

Resonance Raman spectroscopy is a powerful method for studying chromophore structure in BR because one observes vibrational spectra that are sensitive to structural changes and because resonance enhancement of the scattering permits the selective observation of spectra from particular intermediates. By using flow or multiple-pulse, pump-probe configurations it is also possible to obtain time-resolved Raman spectra of the various intermediates. Another advantage is the ability to regenerate the pigment with isotopic derivatives of retinal which enables us to precisely determine the structure of the chromophore (Lugtenburg *et al* 1988).

One simple way of obtaining spectra of transient photochemical intermediates is shown in figure 6. A solution of purple-membrane is allowed to flow through a glass

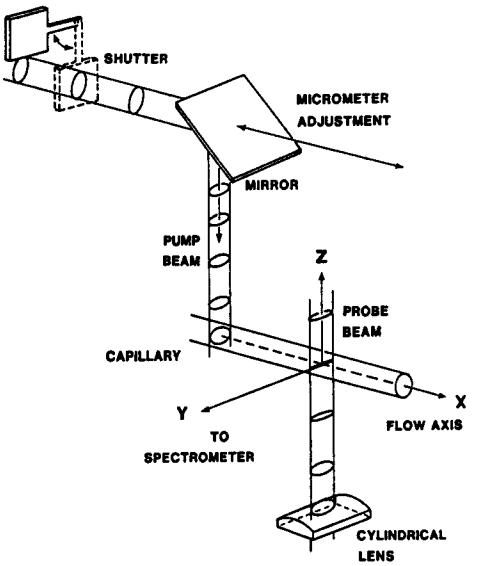

Figure 6. Two-beam flow apparatus for obtaining time-resolved resonance Raman spectra of bacteriorhodopsin.

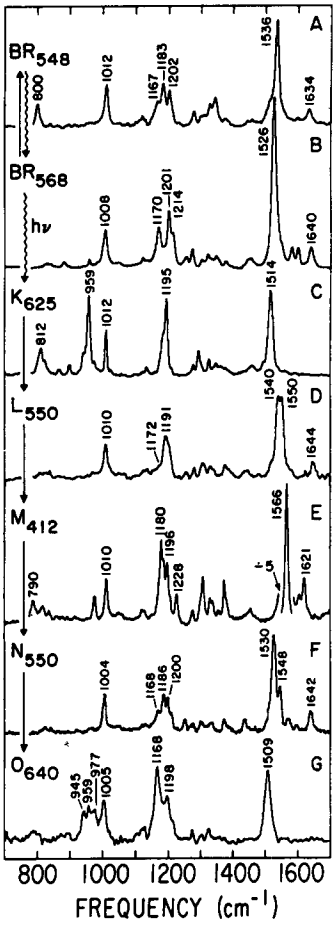

Figure 7. Resonance Raman spectra of bacteriorhodopsin's photochemical intermediates.

capillary and the photochemistry is initiated by an intense pump beam. After a delay time specified by the flow rate and the spacing between the beams, a probe beam is introduced which excites the scattering from the intermediate of interest. The delay time and the probe wavelength are selected to optimize the scattering from the desired intermediate. This method has been used to obtain kinetic resonance Raman spectra of the majority of bacteriorhodopsins's intermediates as shown in figure 7 (Mathies *et al* 1987). It is clear that the Raman spectra for each intermediate are very distinctive. These data have been analyzed with isotopic derivatives of retinal to determine their structure. In summary, the initial transition to form J and K is simply a 13-*trans*→ 13-*cis* transition. The chromophore conformationally relaxes in the K→L isomerization and the Schiff base deprotonates in the L→M transition with no change of chromophore configuration or conformation. Schiff base deprotonation is kinetically associated with proton release to the exterior of the cell. In the M→N transition the Schiff base reprotonates, but reisomerization back to all-*trans* does not occur until O_{640}.

Once the Raman spectrum of each intermediate has been determined, these data can be used as a fingerprint for the concentration of each intermediate in the photocycle.

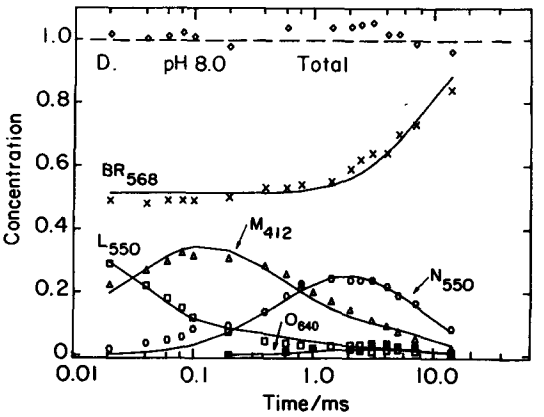

Figure 8. Plot of the concentration of bacteriorhodopsin's photochemical intermediates verses time fit to the kinetic scheme BR ⇒ L ⇔ M ⇔ N ⇒ O ⇒ BR (from Ames *et al* 1990).

This is an important capability because there has been a great deal of controversy about the kinetic scheme that best describes the photocycle (Diller and Stockburger 1988; Dancshazy *et al* 1988; Kouyama *et al* 1988). Kinetic absorption spectroscopy has been unable to resolve this problem because the absorption spectra overlap heavily and are not distinctive. Raman spectroscopy has a clear advantage in addressing this problem because the vibrational spectra are very distinctive. Therefore, we obtained kinetic Raman spectra at a variety of probe wavelengths and analyzed these data using the basis spectra in figure 7. This permitted the determination of the absolute concentrations of the various intermediates as functions of time as shown in figure 8 (Ames and Mathies 1990). With absolute concentrations it is possible to unambiguously refine potential kinetic schemes to fit the observed data. The simplest kinetic scheme that accurately describes these data is a photoreaction cycle which incorporates backreactions between L, M, and N as required by microscopic reversibility (BR → K → L ↔ M ↔ N → O → BR). The incorporation of backreactions accurately reproduces the biphasic rise and decay kinetics observed for L, M, and N (Hanamoto *et al* 1984; Kouyama *et al* 1988) and shows that N is a direct decay product of M (Fodor *et al* 1988). An additional result is the demonstration that proton uptake by the *protein* occurs *after* the chromophore picks up a proton from an internal residue forming N (Ames and Mathies 1990).

4. Molecular model for proton pumping

In figure 9 we present a molecular graphics model for each BR photocycle intermediate to illustrate a molecular mechanism of proton pumping. This model is consistent with the chemical structure of the chromophore determined in the Raman analysis. This structure is essentially identical to that refined to the 3-D electron diffraction data on BR_{568} (Henderson *et al* 1990). The all-*trans* chromophore in BR_{568} is weakly hydrogen-bonded to Asp-212 as shown by linear dichroism studies (Lin and Mathies 1989). It has also been suggested that the ionized Asp-212 and Asp-85 residues are stabilized electrostatically by the nearby Arg-82 (Braiman *et al* 1988; Stern and Khorana 1989).

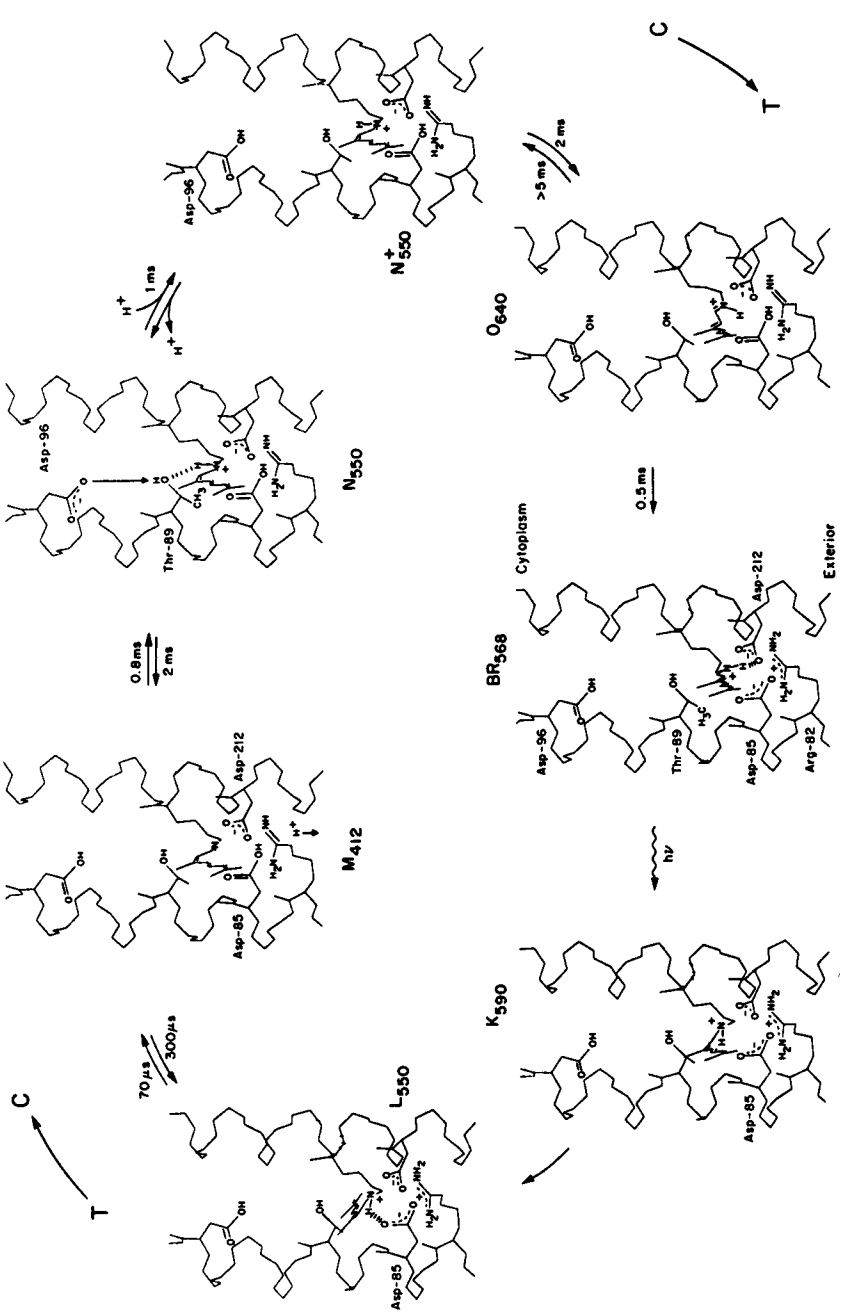

Figure 9. Molecular graphics representation for each of bacteriorhodopsin's photocycle intermediates (Ames *et al* 1990). A side view of helices C and G is shown highlighting residues Asp-85, Arg-82, Thr-89, Asp-96, Asp-212 and Lys-216 and their relation to the retinal chromophore. The indicated times are the reciprocal exponential rate constants for the elementary steps at neutral pH. A two-state protein conformational switch is used to control the connectivity of the Schiff base proton. In the T-state, the binding pocket sterically accommodates the 13-*trans* chromophore and the Schiff base group is connected to exterior residues. In the C-state the pocket accommodates the 13-*cis* chromophore and the Schiff base is connected to cytoplasmic residues.

Photoisomerization to produce K carries the Schiff base away from Asp-212 toward Asp-85. The Schiff base counterion is Asp-85 in K and L_{550}, consistent with observations that substitution of Asp-85 with asparagine eliminates proton pumping activity (Mogi *et al* 1988) and formation of M_{412} (Stern *et al* 1989). During the $K \rightarrow L_{550}$ transition, the 13-*cis* chromophore conformationally relaxes and forms a stronger hydrogen-bond with Asp-85.

In the $L_{550} \rightarrow M_{412}$ transition, the Schiff base proton is transferred to Asp-85. Protonation of Asp-85 initiates the release of a proton to the exterior from Arg-82. The protonation of Asp-85 in M_{412} is clearly evident from the BR → M FTIR difference spectra (Braiman *et al* 1988). A unique aspect of our model is that Schiff base deprotonation is accompanied by a T → C protein conformational change which shifts the Schiff base away from Asp-85 and connects it to a hydrogen-bonded chain or channel that leads to the cytoplasmic surface. The large frequency changes in amide I and II modes in the BR → M FTIR difference spectra provide support for a protein conformational change in M_{412} (Braiman *et al* 1987). The T → C transition is the molecular mechanism for the "reprotonation switch", which allows the 13-*cis* chromophore to donate a proton to Asp-85 (during $L_{550} \rightarrow M_{412}$) and subsequently accept a proton from a cytoplasmic residue during M_{412} decay.

Reprotonation of the Schiff base and cytoplasmic proton uptake by the protein occur in two separate sequential steps which are driven by the net negative charge in the binding sites of M_{412} and N_{550}. During the $M_{412} \rightarrow N_{550}$ transition, Asp-96 donates a proton to the Schiff base via some intermediate group which could be Thr-89 and/or H_2O. The involvement of Asp-96 is based on the observation that substitution of Asp-96 by asparagine dramatically slows down the M_{412} decay (Otto *et al* 1989) and decreases proton pumping activity (Mogi *et al* 1988). In the $N_{550} \rightarrow N^{+}_{550}$ transition, our kinetic studies indicate that there is a protonation of the protein. Since Asp-96 reprotonates during proton uptake from the cytoplasm, it is reasonable to suggest that it protonates in $N_{550} \rightarrow N^{+}_{550}$.

The pump is reset by a reversal of the protein conformation from C → T which drives a concomitant *cis* → *trans* isomerization during $N^{+}_{550} \rightarrow O_{640}$. One of the key features of this model is that photoisomerization of the chromophore drives the protein from its "T conformation" to its "C conformation" thereby storing energy in protein deformation. This stored energy is utilized in the N_{550} to O_{640} transition to drive the chromophore back to the all-*trans* configuration. The weak electrostatic interaction of the positive chromophore with the neutral Asp-85 accounts for the red-shifted λ_{max} in O_{640}. In the $O_{640} \rightarrow BR_{568}$ transition, the positive charge on the chromophore causes Asp-85 to transfer its proton to Arg-82 followed by conformational relaxation to bring the Schiff base group in contact with Asp-212. An intriguing prediction of this model is that if Arg-82 is removed, then proton release to the cell exterior from Asp-85 would be delayed until the $O_{640} \rightarrow BR_{568}$ transition, after proton uptake. This prediction has been dramatically confirmed by the recent work of Otto *et al* (1990) lending support to our molecular mechanism.

Acknowledgements

The work presented here was performed in collaboration with W T Pollard, J B Ames and S W Lin.

References

Ames J B and Mathies R A 1990 *Biochemistry* **29** 7181
Birge R R 1990 *Biochem. Biophys. Acta* **1016** 293
Braiman M S, Ahl P L and Rothschild K J 1987 *Proc. Natl. Acad. Sci. USA* **84** 5221
Braiman M S, Mogi T, Marti T, Stern L J, Khorana H G and Rothschild K J 1988 *Biochemistry* **27** 8516
Dancsházy Zs, Govindjee R and Ebrey T G 1988 *Proc. Natl. Acad. Sci. USA* **85** 6358
Diller R and Stockburger M 1988 *Biochemistry* **27** 7641
Fodor S P A, Ames J B, Gebhard R, van den Berg E M M, Stoeckenius W, Lugtenburg J and Mathies R A 1988 *Biochemistry* **27** 7097
Hanamoto J, Dupuis P and El-Sayed M A 1984 *Proc. Natl. Acad. Sci. USA* **81** 7083
Henderson R, Baldwin J M, Ceska T A, Zemlin F, Beckman E and Downing K H 1990 *J. Mol. Biol.* **213** 899
Khorana H G 1988 *J. Biol. Chem.* **263** 7439
Kosloff R 1988 *J. Phys. Chem.* **92** 2087
Kouyama T, Nasuda-Kouyama A, Ikegami A, Mathew M K and Stoeckenius W 1988 *Biochemistry* **27** 5855
Lin S W and Mathies R A 1989 *Biophys. J.* **56** 653
Lugtenburg J, Mathies R A, Griffin R G and Herzfeld J 1988 *Trends Biochem. Sci.* **13** 388
Mathies R A, Brito Cruz C H, Pollard W T and Shank C V 1988 *Science* **240** 777
Mathies R A, Smith S O and Palings I 1987 *Biological applications of Raman spectroscopy* (ed.) T G Spiro (New York: John Wiley and Sons) pp. 59–108
Mogi T, Stern L J, Marti T, Chao B H and Khorana H G 1988 *Proc. Natl. Acad. Sci. USA* **85** 4148
Otto H, Marti T, Holz M, Mogi T, Lindau M, Khorana H G and Heyn M P 1989 *Proc. Natl. Acad. Sci. USA* **86** 9228
Otto H, Marti T, Holz M, Mogi T, Stern L, Engel F, Khorana H G and Heyn M P 1990 *Proc. Natl. Acad. Sci. USA* **87** 1018
Pollard W T, Brito Cruz C H, Shank C V and Mathies R A 1989 *J. Chem. Phys.* **90** 199
Pollard W T, Fragnito H L, Bigot J Y, Shank C V and Mathies R A 1990a *Chem. Phys. Lett.* **168** 239
Pollard W T, Lee S Y and Mathies R A 1990b *J. Chem. Phys.* **92** 4012
Stern L J, Ahl P L, Marti T, Mogi T, Dunach M, Berkowitz S, Rothschild K J and Khorana H G 1989 *Biochemistry* **28** 10035
Stern L J and Khorana H G 1989 *J. Biol. Chem.* **264** 14202